A New Multiscale Approach to Nuclear Fuel Simulations: Atomistic Validation of the Kinetic Method

Z. Insepov,* J. Rest, G. L. Hofman, A. Yacout
Argonne National Laboratory, 9700 S. Cass Ave., Argonne, IL 60439
A.Yu. Kuksin, G. E. Norman, S. V. Starikov, V. V. Stegailov, A. V. Yanilkin
Joint Institute for High Temperatures of Russian Academy of Sciences
13, Bldg. 2, Izhorskaya Street, Moscow 125412 Russia

ABSTRACT

A key issue for fuel behavior codes is their sensitivity to values of various materials properties, many of which have large uncertainties or have not been measured. Kinetic mesoscale models, such as those developed at Argonne National Laboratory within the past decade, are directly comparable to data obtained from in-reactor experiments. In the present paper, a new multiscale concept is proposed that consists of using atomistic simulation methods to verify the kinetic approach. The new concept includes kinetic rate-equations for radiation damage, energetics and kinetics of defects, and gas/defect-driven swelling of fuels as a function of temperature and burnup. The quantum and classical atomistic simulation methods are applied to increase our understanding of radiation damage and defect formation and growth processes and to calculate the probabilities of elemental processes and reactions that are applicable to irradiated nuclear materials.

KEYWORDS: Multiscale approach; Kinetic rate equations; Ab initio force matching method; molecular dynamics

1. INTRODUCTION

Sustainable nuclear energy production must include a comprehensive analysis of nuclear fuel behavior. Fuel behavior codes are sensitive to materials parameters, many of which have large uncertainties or have not been measured; thus, a complete understanding of radiation damage and swelling of nuclear fuels throughout the operating burnup and temperature regime is required [1, 2].

Safety criteria can be validated in several ways: one is to experimentally test the fuels; another is to develop and benchmark existing analytical and computational models. Several important parameters are the fission gas content at grain boundaries and the porosity that promotes fuel swelling and grain separation during both normal and transient behavior [3].

Much effort has been devoted to replacing highly enriched nuclear fuels with high-density, low enriched (< 20% U^{235}) fuels. Most of the new replacements are directed toward using a U-Mo alloy with 7–10 wt% Mo. Adding Mo mitigates irradiation-induced swelling of pure U fuels at temperature where U transforms to α-phase. Mo is highly soluble in γ-U, and low-temperature U-Mo alloys are considered as promising low-enriched fuels for research and test reactors [4,5]

A vast literature exists on helium and fission gas properties of irradiated body-centered cubic (BCC) metals, including Mo and Mo alloys [6-15]. The most striking feature of the irradiation of metals with energetic ions to high dose is formation of void and/or gas bubble superlattices. Superlattices are periodic void or bubble arrays in metals. In Mo they were first observed by Evans in samples irradiated by 2 MeV nitrogen ions at 870°C [6] and by Sass and Eyre for 36 keV alpha-particle implantation into Mo to a dose of 10^{17} ions/cm^2 at 300K [7]. The mobilities of self-interstitials and vacancies are very low at these temperatures, yet the bubbles were able to nucleate and grow.

* Corresponding author: insepov@anl.gov; Tel: 630-252-5049, Fax: 630-252-5986

The results of neutron irradiations at a fluence of 1×10^{22} n/cm^2 of Mo at six different temperatures in the range 430–-1000°C have been characterized as black spot clusters, loops, rafts, voids and dislocations [8]. The void densities and sizes were characterized as $N_v=3.6\times10^{20}\exp(-26.9\ T/T_m)$, $d_v=1.5\exp(-9.44\ T/T_m)$, where T/T_m is the irradiation temperature as a fraction of the melting point. Interstitials, vacancies, and helium gas atoms contributed to lattice damage; and alignment of helium bubbles was observed in Mo irradiation experiments with helium ions in the range 18 to 60 keV over a wide range of temperatures from 20 to 700°C [9]. The bubble lattice period in the [110] direction was measured to be between 3.2 and 5 nm at temperatures below 700°C. The bubble parameters were insensitive to the vacancy mobility, and the role of interstitials in creation of surface stresses was discussed [9].

Planar-shaped cavities containing helium gas were obtained at low temperatures and transformed into helium bubbles after annealing at temperatures between 600°C and 800°C in fusion environments [10]. The results were interpreted via a helium-vacancy complex formation on {011} planes and by a loop punching mechanism due to overpresurized gas bubbles. The loops were aligned along the glide direction, which is [111] in BCC metals [10,11].

Analysis techniques such as TEM, HRTEM, x-ray diffraction, EELS, and XANES have been discussed in various review papers [12–15]. Characterization of highly pressurized bubbles in liquid or solid form (depending on implantation temperature and fluence) showed that solid bubbles have a face-centered cubic (FCC) or hexagonal close-packed lattice, reflective of the symmetry of the host material [12]. At high pressure and temperature, the solid bubbles transformed into liquid form under the same conditions as bulk solids [12].

The breakup of superlattices in FCC materials leads to more exotic superlattices such as honeycombs and macroscopically large superlattices with periods ~20 times larger than those of the original superlattice [13]. A typical superlattice period is ~5 nm, with a density of 1.8×10^{19} bubbles/cm^3. The ordering of bubbles has been observed to develop subsequent to an initial random distribution of bubbles in the host matrix [14].

Li et al. [15] irradiated polycrystalline Mo at the High Flux Isotope Reactor with neutrons to doses up to 0.28 dpa at 80°C. As-irradiated samples were characterized by resistivity measurements at room temperature, SEM, TEM, and positron annihilation spectroscopy. Tensile tests were conducted for strain rates of 1×10^{-5} – 1×10^{-2} s^{-1}. The authors concluded that cascade clustering of vacancies might be important for radiation damage dynamics in Mo. Neutron irradiation leads to radiation softening at lower neutron doses because of a reduction of the yield stress for increasing strain rate.

Atomistic simulations have been applied to the study of a wide range of processes underlying bubble formation and growth in FCC and BCC metals [16–20]. The rate of lattice swelling increases with an increase in the helium to metal ratio. By using molecular dynamics with an embedded atom potential and an expanding spherical (structureless) potential for helium bubbles, a dislocation network was found to underlie the bubbles instead of prismatic loops that were assumed in earlier models [16].

Radiation cascade damage dynamics creates thermally unstable vacancy clusters via a production bias model leading to a higher-vacancy supersaturation as the stable clusters of self-interstitial atoms (SIAs) preferentially glide one-dimensionally to dislocations and grain boundaries [17,18]. Void nucleation by the biased co-precipitation of SIAs and vacancies was studied, and the Arrhenius plot of the void density vs homologous temperature (T/Tm) was drawn for FCC Cu and BCC Mo based on experimental data. Similar trends were found for bubbles. Trinkaus and Singh [18] also reviewed helium accumulation in metals, bubble nucleation, low- temperature (diffusion- controlled) vs high- temperature (dislocation- controlled) nucleation, heterogeneous nucleation on defects, bubble migration, coarsening,

bubble-to-void transformation, high pressure equation of state of helium, and stability of bubbles under stress.

Linear (1-D) and planar (2-D) void alignment was distinguished by using Monte Carlo simulation methods [19]. The effects of diffusion anisotropy of interstitials ant their clusters on the kinetics and stability of void lattices are discussed in [19,20].

The growth of a single void was studied using molecular dynamics based on Finnis-Sinclair potentials for several BCC metals including Mo in a simulation with up to 128 million atoms [21]. The dislocation punching mechanism was studied as a function of the void growth rate. The BCC void growth results were compared to earlier results obtained for an FCC metal.

Vacancy diffusion coefficients D_v were measured for Mo based on data for the width of the grain boundary void-denuded zone [22,23]:

$$D_v = D_{vo}\exp(-E_v^m / kT), \quad (1)$$

where the pre-exponential was fitted to experiment as $D_{v0}=1\times10^{-4}$ cm^2/s, the vacancy migration energy was obtained to be E_{mv} = (1.26 ± 0.5) eV in excellent agreement with the theory [24], and experimental values were used for E_{mv} = (1.62 ± 0.27) eV [25].

Although evidence exists that supports the mechanism of self-diffusion in BCC metals at low temperature as substantially based on SIA migration, there is still a great lack of understanding of the migration mechanisms of SIA in BCC metals.

Recently, there has been significant progress in understanding radiation defect agglomeration and dissolution under high damage rates in metals (see, e.g., [26]). However, a similar level of understanding of elemental damage processes and defect evolution crucial for the analysis of nuclear fuels is still missing.

The aim of this paper is to discuss the results of a new methodology being developed at Argonne that will logically connect various scales of simulation starting from ab initio and atomistic molecular dynamics/Monte Carlo (MD/MC) to kinetic rate theory and classical nucleation theory and to experimental verification of basic theoretical models.

An attempt to build a similar multiscale approach was undertaken by Stoller and Greenwood in 1998 where they proposed using MD-simulated cross-sections and hand-shaking and handing-off data to a kinetic microstructural model [27].

2. ATOMISTIC MODELS FOR KINETIC METHOD

An interatomic potential of the embedded atom model (EAM) type is constructed for pure Mo by means of the force matching method [28, 29]. The main idea of the method is fitting the potential to ab initio atomic forces for a set of atomic configurations of different structures. In our work a dataset of atomic forces is generated with density-functional calculations performed with the VASP code [30], taking into account a number of structures with interstitials of several types and vacancies. It enables the reproduction of relative energies of the defects in accordance with the ab initio calculations, which is important for a correct mechanism of their migration [31]. While Derlet et al. constructed a potential of this kind [31], that work describes a thermal expansion and a cold curve of pure Mo and cannot be used for simulating high-energy collision cascades.

The interaction potential between two Xe atoms was obtained by fitting a Morse potential function to the Xe+-Xe potential curves obtained by ab initio calculations in Ref. [32]:

$$U = D_0\left[e^{-2\alpha(r-r_0)} - 2e^{-\alpha(r-r_0)}\right] \quad (2)$$

The following parameters of the Morse function shown in Eq. (2) were used: D_0 = 1.3 eV, α = 1.3 Å^{-1}, r_0 = 3.1 Å, and a cutoff distance of 7Å. Figure 1 shows the fit of the above Morse function to the calculated ab initio data.

A new Morse-type Xe-Mo interatomic potential was developed by comparison of the calculated sputtering yield of Xe ions with extensive experimental data existing for scattering of Xe+ ions from Mo surfaces [33–38]. Two sets of potential parameters were used in our MD calculations. In set #1: D_0 = 23.7 eV, α = 3.95 Å^{-1}, r_0 = 1.9 Å; in set #2: D_0 = 10eV, α = 6 Å^{-1}, r_0 = 1.9 Å, and a cutoff distance r_{cut}=3Å. Figure 2 shows the plot of the Morse potential for the parameter set #2.

Figure 3 compares the sputtering yields for Xe+ ion bombardment of a Mo (100) surface calculated in the present paper with the experimental data obtained from the literature [33–38]. The parameters for the potential function for set #1 yield data close to experiment at higher energies, namely, E~100 eV. However, the calculated yields are much higher than the data at energies lower than 60 eV. Set #2 gives calculated yields close to experiment for both high and low energy regions.

In what follows, the potential using set #2 was applied for studying Xe-bubble properties in Mo. The Mo-Mo EAM potential presented in this work reproduces the cold curve in agreement with the experimental data up to approximately 600 GPa (corresponding compression $V/V_0 \sim 0.5$). In addition, the description of thermal expansion is replicated well up to the melting point. The most stable configurations of interstitial defects are <111> dumbbell and <111> crowdion with very small differences in formation energies. This configuration provides for one-dimensional migration of self-interstitial atoms at very low temperatures [39] in agreement with the resistivity recovery measurements following electron irradiation [40]. With increasing temperature the <111>-<110> dumbbell transitions are activated, providing a rotation of the axis of migrating crowdions, and hence providing a basis for a viable mechanism for three-dimensional diffusion.

The structure and mobility of self-interstitial defects, vacancies, and dislocations in molybdenum have been studied with the classical molecular dynamics model. An attempt has been made to represent the results of the simulations as constitutive relations for the rate-theory-based models (such as [41]) that have been used to investigate the nucleation and growth of cavities during irradiation and subsequent radiation damage (e.g., that leading to swelling).

Diffusion coefficients were calculated according to eq. (3), relating the accumulation of stochastic displacement of a particle in a time unit with the microscopic diffusion coefficient that can be calculated via molecular dynamics:

$$D = \frac{1}{6}\lim_{t\to\infty}\frac{d\left\langle\left|\vec{r}(t)-\vec{r}(0)\right|^2\right\rangle}{dt} \quad , \qquad (3)$$

where r(0), r(t) are the radius-vectors of the particles and D is the diffusion coefficient. The diffusion coefficients were calculated by using large-scale MD simulations. Fast parallel calculations were carried out on a Blue Gene supercomputer by using a Lammps MD simulation package [42]. A typical MD simulation of a system containing 22,000 Mo atoms in 10 ns was completed in six hours of computing time.

Figure 4 shows a comparison of the results of our MD simulations with the existing experimental data for nonirradiated Mo samples [23, 43–45]. The following experimental data are shown: the self-diffusion coefficients of pure single crystal and polycrystalline Mo [43, 44], the surface diffusivity of Mo containing open surfaces and grain boundaries [23,45]. The calculated results obtained for pure Mo (open circle) are in good agreement with the experimental data reported by Maier et al. [43]. The activation energy for the Mo self-diffusion coefficient in a sample containing voids and vacancies (open

diamonds) is in close agreement with surface diffusion coefficient data measured by Allen et al. [45]. The activation energy of Mo self-diffusion in a sample with Xe-bubbles (open squares) is similar to experimental data obtained by Askill et al. measured for polycrystalline Mo [44].

Thermally activated mobilities of a number of defects have been analyzed over a wide range of temperatures. Diffusion coefficients and the frequencies of rotation of the axis of migrating crowdions have been evaluated from molecular dynamic simulations. This evaluation enables analysis of the effects of diffusion anisotropy on the evolution of the void subsystem, which is assumed to be the origin of the formation of void lattices during irradiation [19,20].

The results for diffusivity of atoms due to vacancies and interstitials that is physically equivalent to the tracer diffusion coefficient in a pure crystal $D_t = f D_\alpha$ (f is the correlation factor [46]) are presented in Fig. 5. Corresponding activation energies can be estimated as 0.97 eV for vacancies and 0.15 eV for interstitials.

Interaction of dislocations with voids and point defects in Mo were studied in both static (energy minimization) and dynamic models, and the results were compared with estimates from dislocation theory. The drag coefficient for dislocations in such systems was then evaluated. Critical stresses for void growth via emission of dislocation loops were estimated as a function of temperature. The detailed results of the dislocation interaction with defects will be published elsewhere. We conclude that molecular dynamics simulations with DFT-based potentials are useful in verifying kinetic models and for evaluating kinetic coefficients.

3. ATOMISTIC VALIDATION OF THE KINETIC METHOD

The primary components of a kinetic theory for the biased and gas-driven swelling of fuels [41] are mechanistic rate-theory-based models for the nucleation and growth of cavities during irradiation. The models include the interaction of the fission gas and gas-filled bubbles with irradiation-induced dislocation loops. The kinetic approach allows direct comparison of the analysis with experimental data [3–5, 41].

The following equations are two of a large set of equations representing the kinetic methodology and describe the evolution of the vacancy and interstitial concentrations during irradiation:

$$\frac{dc_v}{dt} = K - \alpha_r c_v c_i - k_v D_v c_v - 2\Omega^{1/3} b_v D_v c_v n_l / \pi d_l,$$
$$\frac{dc_i}{dt} = K - \alpha_r c_v c_i - k_i D_i c_i - \sqrt{2} D_i c_i c_i / \Omega^{2/3} + 2\Omega^{1/3} b_v D_v c_v n_l / \pi d_l. \quad (4)$$

In these equations, K is the damage rate in *dpa*/*s* α_r is the vacancy recombination coefficient; b_v and Ω are the Burgers vector and atomic volume, respectively; D_v, D_i, and D_g are the vacancy, interstitial, and gas-atom diffusivities, respectively; and k_α ($\alpha = v$, i) are the vacancy and interstitial sink strengths. The k_α include fission gas bubbles, Frenkel pairs, clusters, and dislocations. Similar equations can be written for Frenkel pairs, clusters, dislocation loops, and gas atoms and bubbles.

Figure 6 shows a comparison of the calculated fission gas bubble distribution function for three volume diffusion coefficients. This figure shows the dependence of the calculated bubble-size distribution on the value of D_{vol} for a gas solubility of 2.5 x10^{-8} compared with the measured quantities. As seen from Fig. 6, the value of D_{vol} has a reasonably strong effect on the calculated distribution.

To apply the proposed concept to nuclear fuels at high burnups, one needs the gas atom and gas bubble diffusion coefficients and the interaction mechanisms of fission gas bubbles via dislocation emission and

capture. Multiscale simulation studies to obtain these quantities have been carried out at Argonne in close collaboration with researchers from Russia; the results will be presented elsewhere.

SUMMARY

Kinetic mesoscale models, such as those developed at Argonne National Laboratory are directly comparable to reactor experiments. In our previous work, we successfully applied MD and MC to the calculation of kinetic coefficients for cluster formation processes in rarefied gas and in dense media [47].

In the present paper, a new multiscale concept is proposed that consists of using atomistic simulation methods, verified with experimental data, in order to validate the kinetic approach as a universal tool. Our new concept is based on kinetic rate-equations for radiation damage, energetics and kinetics of defects, and swelling of fuels as a function of temperature and burnup. Quantum and classical atomistic simulation methods are applied to increase our understanding of radiation damage and defect formation and growth processes and to calculate the probabilities of elemental processes and reactions applicable to irradiated nuclear materials. Since the interaction potentials are critical for the new concept, they were developed based on a force-matching method data from ab initio calculations or were fitted to existing experimental data.

As an example of such an approach, EAM potentials for BCC metals were obtained, and a Xe-Mo potential was parameterized via comparison of the calculated sputtering yield of a Mo-surface bombarded with Xe ions with experimental data. Diffusion in irradiated Mo was studied for voids and Xe-bubbles and compared to unirradiated Mo. The diffusion coefficients for SIA, V, and crowdions in BCC metals were calculated for several EAM potentials. Good comparisons between calculated, ab initio, and experimental data were obtained. Thermodynamic, elastic, and defect (I,V, crowdion) properties in BCC metals also were calculated for several new EAM potentials.

ACKNOWLEDGMENTS

This work was supported in part by the Office of Advanced Scientific Computing Research, Office of Science, U.S. Department of Energy, under Contract DE-AC02-06CH11357.

REFERENCES

[1] Nuclear Fuel Safety Criteria. Technical Review, NEA/CSNI/R(99)25, p. 45.
[2] J. Spino, D. Papaioannou, Lattice parameter changes associated with the rim-structure formation in high burn-up UO_2 fuels by micro x-ray diffraction, J. Nucl. Mater. 281 (2000) 146-162.
[3] G.L. Hofman, Y.S. Kim, A classification of uniquely different types of nuclear fission gas behavior, Nucl. Engin. Techn. 37 (2005) 299-308.
[4] S.L. Hayes, M.K. Meyer, G.L. Hofman, R.V. Strain, in Proc.21st Intern. Meet.ing on Reduced Enrichment for Research and Test Reactors (RERTR), Sao Paolo, Brazil, 1998.
[5] S. Van den Berghe, W. Van Renterghem, A. Leenaers, Transmission electron microscopy investigation of irradiated U-7 wt% Mo dispersion fuel, The RERTR-2007 Intern. Meeting on reduced enrichment for research and test reactors, Sept. 23-27, 2007, Prague, Czech Republic.
[6] J.H. Evans, Observations of a regular void array in high purity molybdenum and T.Z.M. irradiated at high temperatures with 2MeV nitrogen ions, Rad. Eff. 10 (1971) 55-60.
[7] S.L. Sass, B.L. Eyre, Diffraction from void and bubble arrays in irradiated Molybdenum, Phil. Mag. 27 (1973) 1447-1453.
[8] V.K. Sikka, J. Moteff, Damage in neutron-irradiated molybdenum, J. Nucl. Mater. 54 (1974) 325-345.
[9] D.J. Mazey, B.L. Eyre[a], J.H. Evans, S.K. Erents, G.M. McCracken, A transmission electron microscopy study of molybdenum irradiated with helium ions, J. Nucl. Mater. 64 (1977) 145-156.
[10] J.H. Evans, A. van Veen, L.M. Caspers, Formation of helium platelets in molybdenum, Nature 291 (1981) 310-311;
[11] J.H. Evans, A. van Veen, L.M. Caspers, The application of TEM to the study of helium cluster nucleation and growth in molybdenum at 300K, Rad. Eff. 78 (1983) 105-120.
[12] K. Krishan, Ordering of voids and gas bubbles in radiation environments, Rad. Eff. 66 (1982) 121-155.
[13] C. Templier, Inert gas bubbles in metals: a review, in Fundamental Aspects of Inert Gases in Solids, Ed. S.E. Donnelly and J.H. Evans, Plenum Press, NY, 1991, 117-132.
[14] P.B. Johnson, Gas bubble lattice in metals, ibid, 167-184.
[15] M. Li, et al, Low temperature neutron irradiation effects on microstructure and tensile properties of molybdenum, J. Nucl. Mater. 376 (2008) 11-28.
[16] S.M. Foiles, J.J. Hoyt, Computer simulation of bubble growth in metal due to He, SAND2001-0661, 2001.
[17] H. Trinkaus, B.N. Singh, Modeling of void nucleation under cascade damage conditions, J. Nucl. Mater. 307-311 (2002) 900-906.
[18] H. Trinkaus, B.N. Singh, Helium accumulation in metals during irradiation – where do we stand?, J. Nucl. Mater. 323 (2003) 229-242.
[19] J.H. Evans, Simulations of the effects of 2-D interstitial diffusion on void lattice formation during irradiation, Phil. Mag. 86 (2006) 173-188.
[20] A.A. Semenov, C.H. Woo, W. Frank, Diffusion anisotropy and void development under cascade irradiation, Appl Phys A. 93 (2008) 365–377.
[21] R. Rudd, Void growth in BCC metals simulated with molecular dynamics using the Finnis-Sinclair potential, Phil. Mag. 89 (2009) 3133-3161.
[22] Yu.V. Konobeev, A.V. Subbotin, V.N. Bykov, V.I. Tscherbak, Grain boundary void denuded zone in irradiated metals, Phys. Stat. Sol. A 29 (1975) K121.

[23] Yu.V. Konobeev, V.I. Tscherbak, V.N. Bykov, A.V. Subbotin, Determination of the vacancy diffusivity in Molybdenum and Nickel from data on the width of the grain boundary void denuded zone, Phys. Stat. Sol. A 40 (1977) K89.
[24] R.A. Johnson, W.D. Wilson, Proc. Intern. Conf. Interatomic Potential and Simulation of Lattice Defects, Plenum Press, NY 1972, p. 301.
[25] M. Suezawa, H. Kimura, Phil. Mag. 28 (1973) 901.
[26] Yu. N. Osetsky, D.J. Bacon, A. Serra, B.N. Singh, S.I. Golubov, Stability and mobility of defect clusters and dislocation loops in metals, J. Nucl. Mater. 276 (2000) 65-77.
[27] R.E. Stoller, L.R. Greenwood, From molecular dynamics to kinetic rate theory: A simple example of multiscale modeling, ORNL/CP-10122, Proc. of Materials Research Society 1998 Fall Meeting, Boston, 1998.
[28] F. Ercolessi, J.B. Adams, Interatomic Potentials from First-Principles Calculations: the Force-Matching Method, Europhys. Lett. 26 (1994) 583.
[29] P. Brommer, F. Gähler, Potfit: Effective potentials from ab-initio data, Modelling Simul. Mater. Sci. Eng. 15(2007) 295–304.
[30] G. Kresse, J. Furthmuller, Efficient iterative schemes for ab initio total-energy calculations using a plane-wave basis set, Phys. Rev. B 54 (1996) 11 169.
[31] P.M. Derlet, D. Nguyen-Manh, S.L. Dudarev, Multiscale modeling of crowdion and vacancy defects in body-centered-cubic transition metals, Phys. Rev. B 76 (2007) 054107.
[32] I. Paidarova, F.X. Gadea, Accurate ab-initio calculation of potential energy curves and transition dipole moments of the Xe2+ molecular ion, Chem. Phys. 274 (2001) 1-9.
[33] C.H. Weijsenfeld, A. Hoogendoorn, M. Koedam, Sputtering of polycrystalline metals by inert gas ions of low energy (100-1000 eV), Physica 27 (1961) 763.
[34] D. Rosenberg, G.K. Wehner, Sputtering yield for low energy He+, Kr+, and Xe+ bombardment, J. Appl. Phys. 33 (1962) 1842.
[35] J.J. Blandino, D.G. Goodwin, C.E. Garner, Low energy sputter yields for diamond, carbon-carbon composite, and molybdenum subject to xenon ion bombardment, Diamond and Related Materials, 9 (2000) 1992-2001.
[36] R.P. Doerner, D.G. Whyte, D.M. Goebel, Sputtering yield measurements during low energy xenon plasma bombardment, J. Appl. Phys. 93 (2003) 5816.
[37] R. Kolasinski, Oblique angle sputtering yield measurements for ion thruster grid materials, AIAA Paper No. 2005-3526, 2005.
[38] E. Oyarzabal, J. H. Yu, R.P. Doerner, G.R. Tynan, K. Schmid, Molybdenum angular sputtering distribution under low energy xenon ion bombardment, J. Appl. Phys. 100 (2006) 063301.
[39] S.P. Fitzgerald, D. Nguyen-Manh, Peierls potential for crowdions in the BCC transition metals, Phys. Rev. Lett. 101 (2008) 115504.
[40] P. Ehrhart, P. Jung, H. Shultz, H. Ullmaier, Atomic Defects in Metals, ed. by H. Ullmaier Landolt-Bornstein New Series, Group III, Vol. 25 (Springer-Verlag, Berlin, 1991).
[41] J. Rest, G.L. Hofman, An alternative explanation for evidence that xenon depletion, pore formation, and grain subdivision begin at different local burnups, J. Nucl. Mater. 277 (2000) 231-238
[42] S. J. Plimpton. Fast parallel algorithms for short-range molecular dynamics, J. Comp. Phys. 117 (1995) 1–19.
[43] K. Maier, H. Mehrer, and G. Rein, Self-diffusion in molybdenum, Zeitschrift fuer Metallkunde, 70 (1979) 271.
[44] J. Askill, D.H. Tomlin, Self-diffusion in molybdenum, Phil. Mag. 8 (1963) 997-1001.

[45] B.C. Allen, The surface self-diffusion of Mo, Cb (Nb), and Re, Metallurgical Trans. 3 (1972) 2544-2547.
[46] N. Soneda, T. Diaz de la Rubia, Defect production, annealing kinetics and damage evolution in α-Fe: An atomic-scale computer simulation, Philos. Mag. A 78 (1998), 995-1019]
[47] Z. Insepov, E.M. Karataev, G.E. Norman, The kinetics of condensation behind the shock front, Z. Phys. 20 (1991) 449-451.

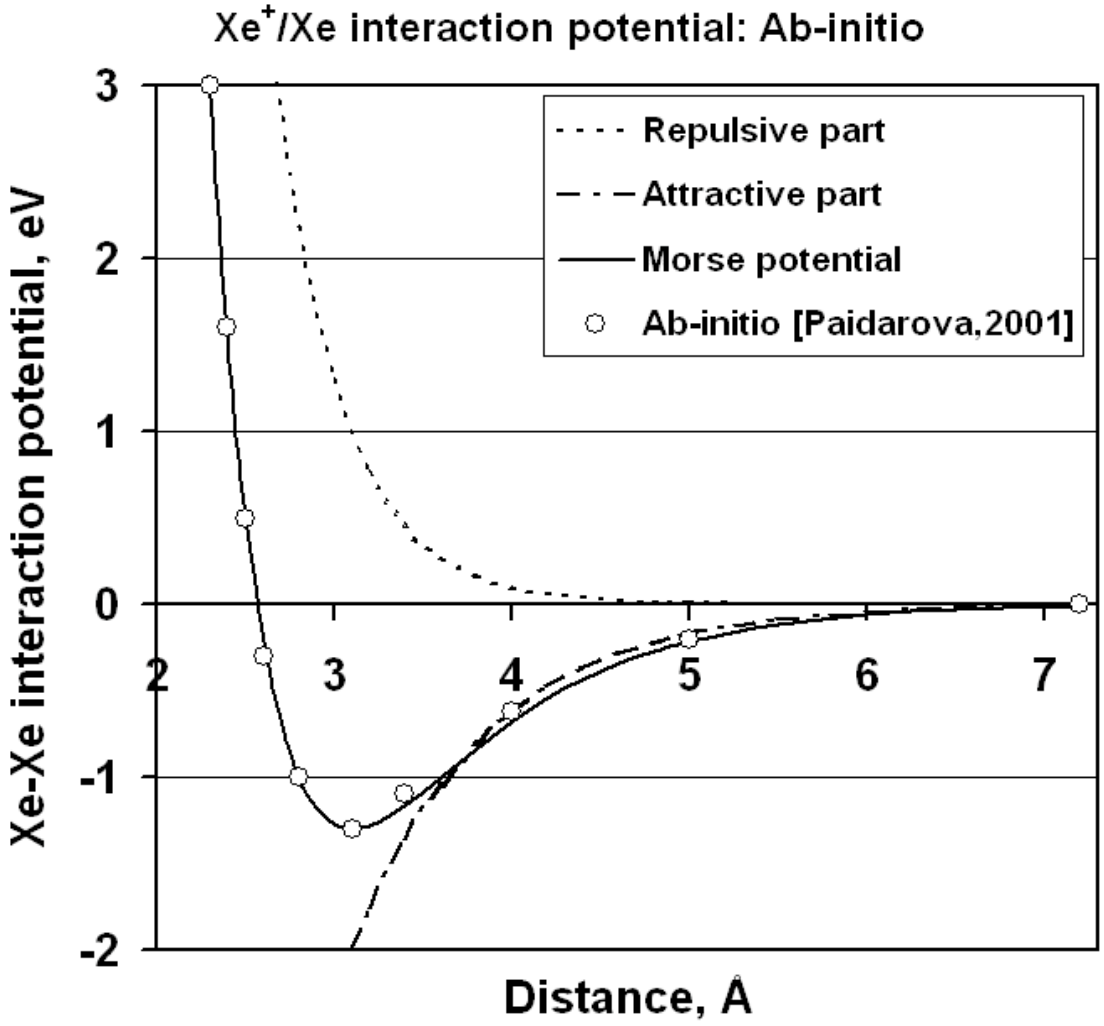

Figure 1

Xe-Xe potential was fitted to an ab initio calculation published in Ref. [32].

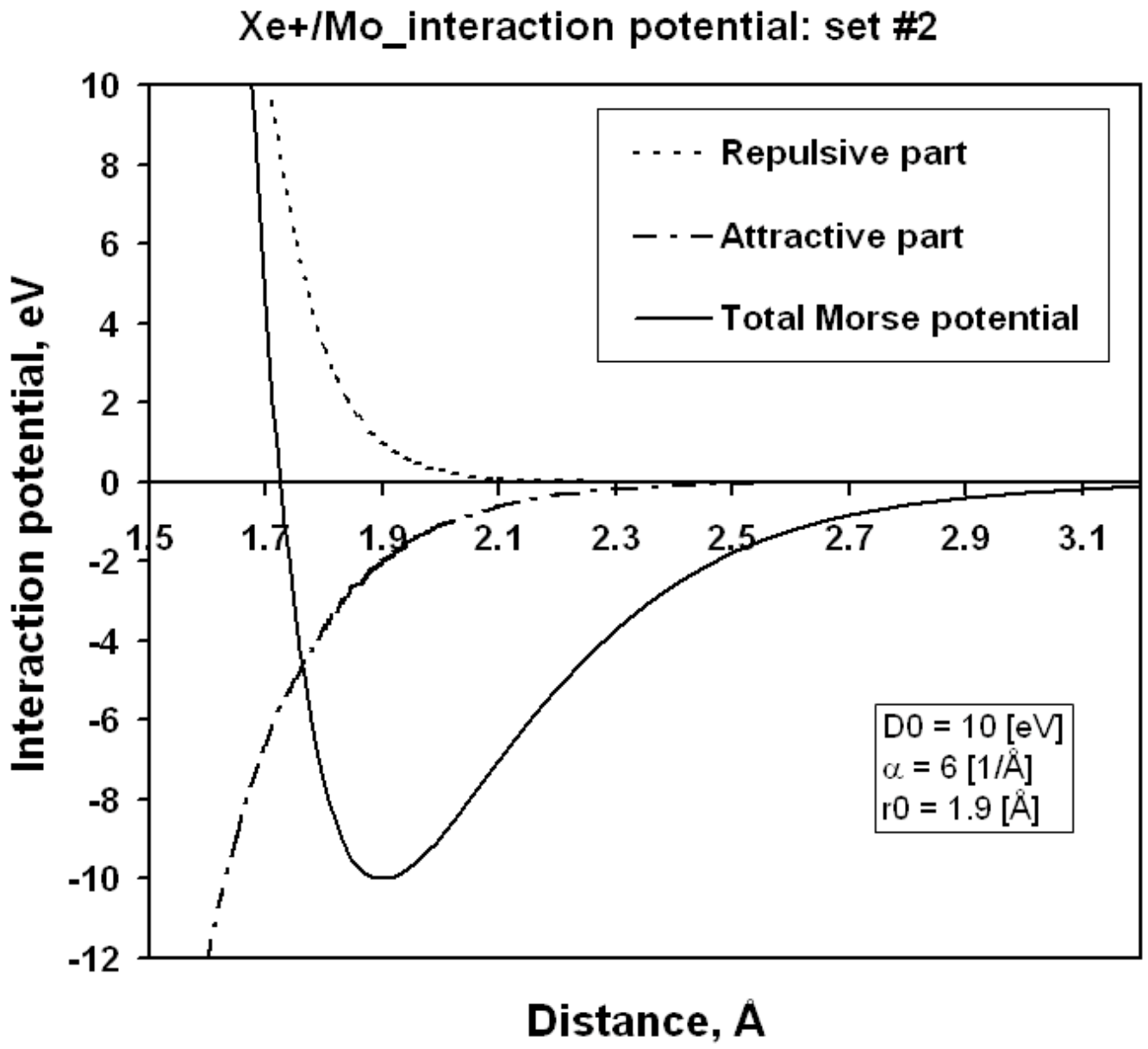

Figure 2

Xe-Mo potential was obtained by MD calculation of the sputtering yield of a Mo surface by low-energy Xe-ions that were fitted to the experimental data for surface erosion of Mo [33–38].

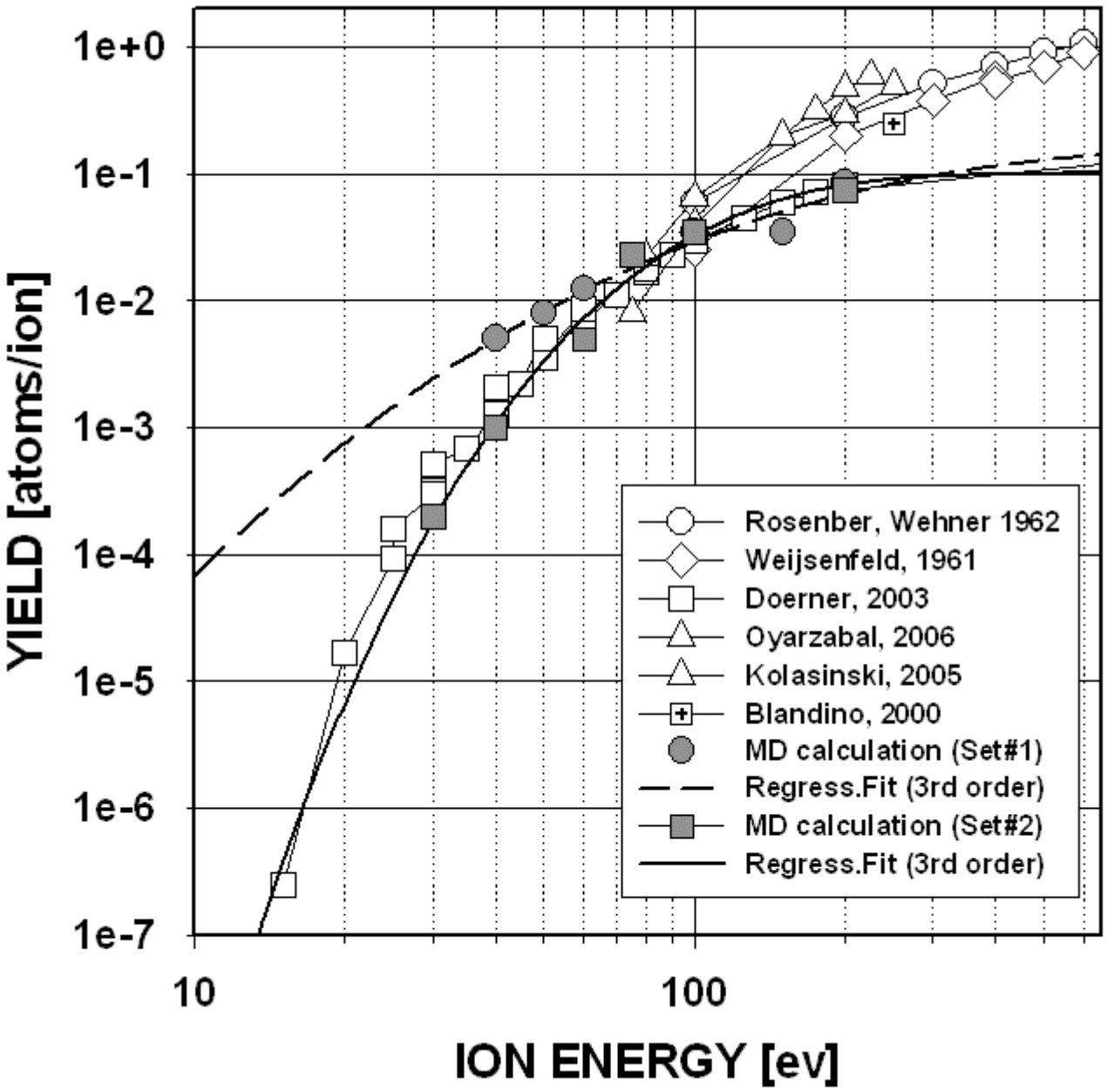

Figure 3

Comparison of the sputtering yield of a Mo (100) surface bombarded by accelerated Xe+-ions interacting with Mo atoms via a Morse potential with the experimental data from Refs. [33–38] (see also Fig. 2).

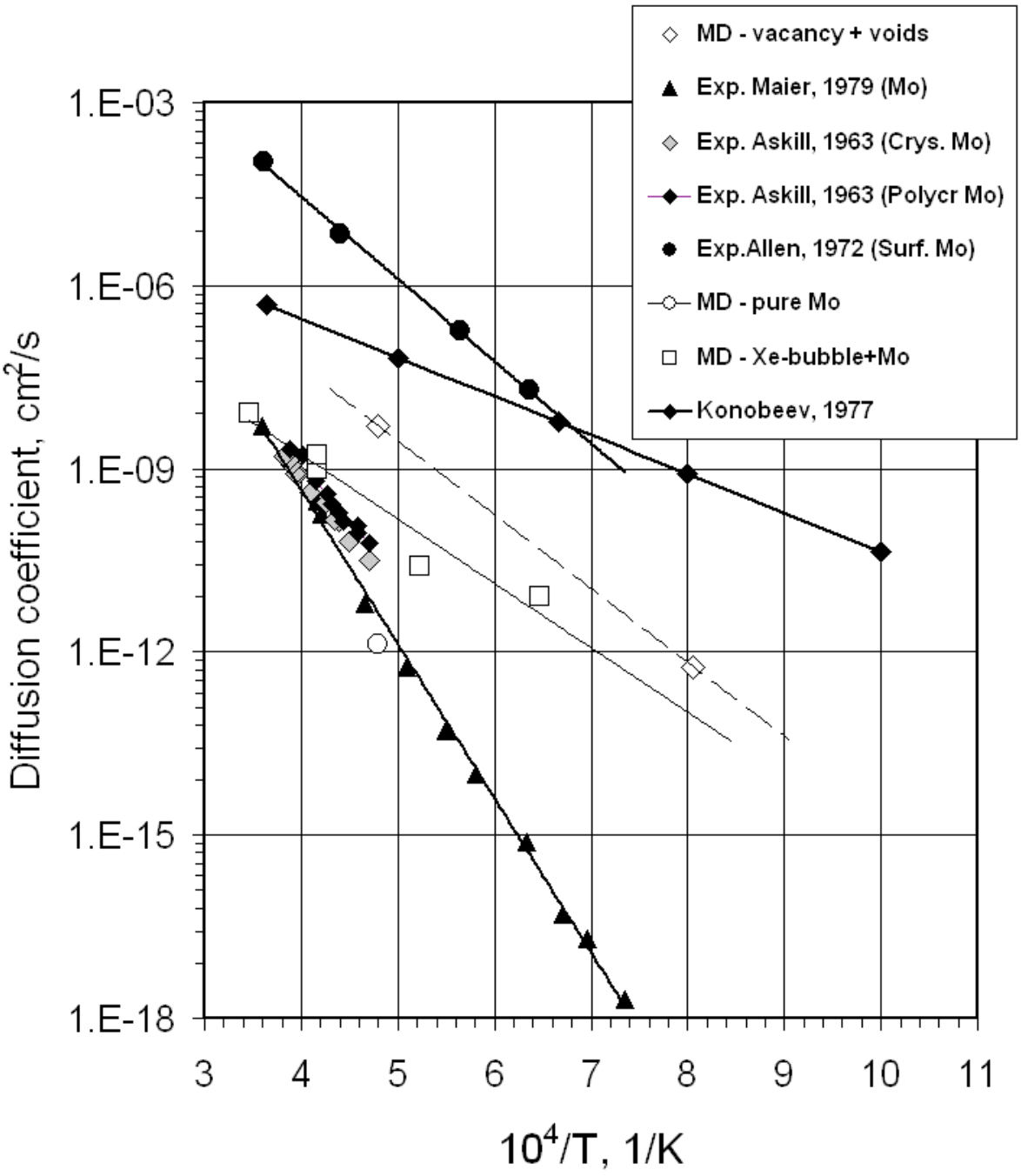

Figure 4

Mo and Xe diffusion coefficients calculated in this paper (open symbols) and compared to existing experimental data [23,43–45]. Solid symbols are the experimental data for self-diffusion coefficients in a single-crystal Mo (solid triangles) [43] and polycrystalline Mo (solid diamonds) [44] and surface diffusion coefficient of Mo (solid circles) [45].

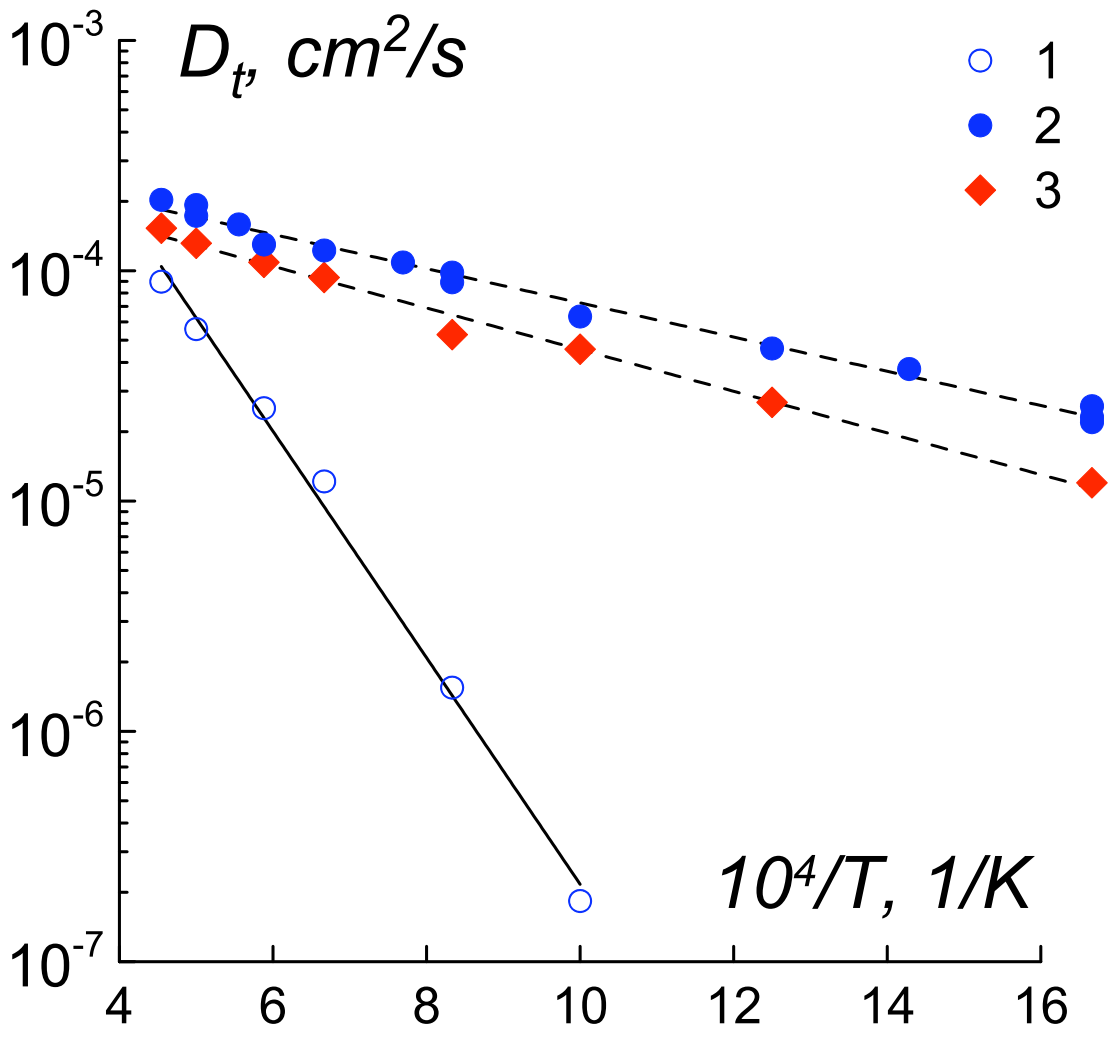

Figure 5

Arrhenius plot of the diffusion coefficients of the tracers for (1) vacancies, potential from this work; (2) interstitials, potential from this work; and (3) interstitials, potential [31].

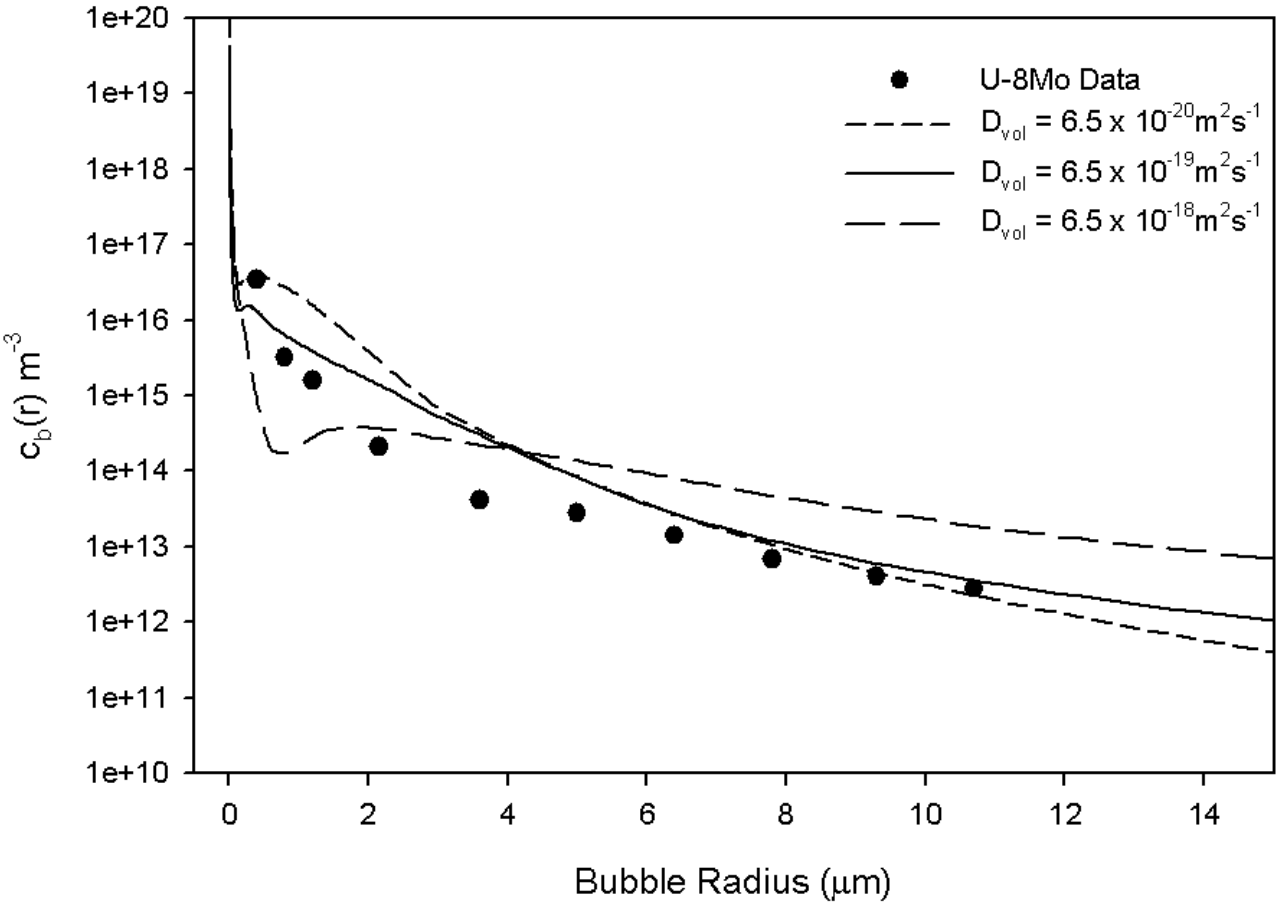

Figure 6

Calculated bubble-size distributions for an irradiation in U-8Mo at 850K to 4% U atom burnup using eq. (4) and the multiatom nucleation model for three values of the rare-gas solubility compared with irradiation data.

Figure Captions

Figure 1. Xe-Xe potential was fitted to an ab initio calculation published in Ref. [32].

Figure 2. Xe-Mo potential was obtained by MD calculation of the sputtering yield of a Mo surface by low-energy Xe-ions that were fitted to the experimental data for surface erosion of Mo [33–38].

Figure 3. Comparison of the sputtering yield of a Mo (100) surface bombarded by accelerated Xe+-ions interacting with Mo atoms via a Morse potential with the experimental data from Refs. [33-38] (see also Fig. 2).

Figure 4. Mo and Xe diffusion coefficients calculated in this paper (open symbols) and compared to existing experimental data [23,43-45]. Solid symbols are the experimental data for self-diffusion coefficients in a single-crystal Mo (solid triangles) [43] and polycrystalline Mo (solid diamonds) [44] and surface diffusion coefficient of Mo (solid circles) [45].

Figure 5. Arrhenius plot of the diffusion coefficients of the tracers for (1) vacancies, potential from this work; (2) interstitials, potential from this work; and (3) interstitials, potential [31].

Figure 6. Calculated bubble-size distributions for an irradiation in U-8Mo at 850K to 4% U atom burnup using eq. (4) and the multiatom nucleation model for three values of the rare-gas solubility compared with irradiation data.